Vol. 12, pp. 21–29 (2015)
doi: 10.2142/biophysico.12.0_21

Biophysics and Physicobiology

https://www.jstage.jst.go.jp/browse/biophysico/

Regular Article

The molecular dynamics of crawling migration in microtubule-disrupted keratocytes

Hitomi Nakashima[1], Chika Okimura[1] and Yoshiaki Iwadate[1]

[1]*Faculty of Science, Yamaguchi University, Yamaguchi 753-8512, Japan*

Received May 18, 2015; accepted July 24, 2015

Cell-crawling migration plays an essential role in complex biological phenomena. It is now generally believed that many processes essential to such migration are regulated by microtubules in many cells, including fibroblasts and neurons. However, keratocytes treated with nocodazole, which is an inhibitor of microtubule polymerization – and even keratocyte fragments that contain no microtubules – migrate at the same velocity and with the same directionality as normal keratocytes. In this study, we discovered that not only these migration properties, but also the molecular dynamics that regulate such properties, such as the retrograde flow rate of actin filaments, distributions of vinculin and myosin II, and traction forces, are also the same in nocodazole-treated keratocytes as those in untreated keratocytes. These results suggest that microtubules are not in fact required for crawling migration of keratocytes, either in terms of migrating properties or of intracellular molecular dynamics.

Key words: actin retrograde flow, cell migration, cell shape, focal adhesions, traction forces

Cell-crawling migration plays an essential role in complex biological phenomena, including development [1–3], wound healing [4,5], immune system function [6] and cancer metastasis [7]. It is at present generally believed that extension of the leading edge that is induced by actin polymerization (AP) [8,9] and retraction of the rear by actomyosin contraction [10,11] are the driving forces of cell-crawling migration. Microtubules have been thought to play an essential role in cell migration since observations of the inhibition of fibroblast migration by the application of colcemid, a microtubule depolymerizing drug [12]. It is now generally believed that numerous processes essential to AP and actomyosin contraction are regulated by microtubules, and depend on distinct modes of microtubule dynamics [13,14]. In the front of the cell, the small Rho GTPase Rac1 is thought to coordinate Arp2/3 and formin-dependent actin nucleation [15]; and in the rear, RhoA activates myosin II through Rho kinase (ROCK) activation and generates contractility [16]. Microtubule polymerization activates Rac1 [17] through the activation of TIAM1 [18] or STEF (TIAM2) [19], while microtubule depolymerization promotes RhoA activation [20–22] through the activation of GEF-H1 (Lfc) [23].

Fish epidermal keratocytes are a widely used cell type in the study of the mechanics of cell crawling migration. They have a spindle-shaped cell body and a large crescent-shaped lamellipodium filled with actin filaments (F-actin). They do not change their overall shape during crawling migration [24], indicating that the rate of leading-edge expansion is highly organized in time and space. Migrating keratocytes rarely generate cytoplasmic fragments spontaneously in culture [25]. Fragmentation can be induced in almost every cells by treatment with the protein kinase inhibitor staurosporine [26]. Cytoplasmic fragments maintain their migratory behavior for more than 1 hour in a pattern indistinguishable from that of intact cells, in spite of the fragments containing no nuclei, microtubules or centrioles [25,26]. Keratocytes treated with nocodazole also migrate at the same velocity and with the same directionality as untreated cells [25]. These observations suggest that microtubules are not necessarily required for crawling migration of keratocytes, at least

Corresponding author: Yoshiaki Iwadate, Faculty of Science, Yamaguchi University, Yamaguchi 753-8512, Japan.
e-mail: iwadate@yamaguchi-u.ac.jp

from the viewpoint of migration properties.

In this study, we compared not only the migration properties such as velocity, directionality and the shape of the leading edge, but also the molecular dynamics that regulate migration, such as retrograde F-actin flow (RF) rate, distributions of focal adhesions and myosin II, and traction forces between keratocytes treated with or without nocodazole. There was no significant difference in any of them, suggesting that microtubules are not required for crawling migration of keratocytes, and are not an essential part of intracellular molecular dynamics.

Materials and methods

Cell culture

Keratocytes from the scales of the Central American cichlid (*Theraps nicaraguense*) were cultured as described previously [27,28]. Briefly, fish scales were extracted and washed in culture medium – Leibovitz's Medium (L-15, L5520; Sigma-Aldrich, St Louis, MO) supplemented with 10% fetal calf serum (Nichirei, Tokyo, Japan) and antibiotic/antimycotic solution (09366-44; Nacalai tesque, Kyoto, Japan). The scales were placed external side up on the bottom of a chamber, the floor of which comprised a coverslip, then covered with another small coverslip and allowed to adhere to the bottom coverslip for 1 h at room temperature. Then, after removal of the upper coverslip, culture medium was added to the chamber and the scales were kept at room temperature again overnight to allow the cells to spread from the scale. Cells were washed briefly with Dulbecco's phosphate-buffered saline without Ca^{2+} and Mg^{2+} (PBS--) and then treated with 0.5 g/l trypsin and 0.53 mM EDTA in PBS (trypsin-EDTA, 32778-34; Nacalai tesque, Kyoto, Japan) for 30–60 seconds. The trypsin was quenched with a ten-fold excess of culture medium.

Nocodazole treatment

Nocodazole (487928; Calbiochem, San Diego, CA) was dissolved at 10 mg/ml in DMSO and then diluted 1,000 times with the culture medium. This nocodazole medium was applied to the chamber, to whose bottom cells had adhered, just after the removal of the medium in which they had been immersed beforehand. After 30 min, cells in the chamber were used for experiments without removal of nocodazole and will henceforth be referred to as "nocodazole-treated cells." The cells treated with only 0.1% DMSO were used in the control experiments and will henceforth be referred to as "untreated cells."

Loading of Alexa phalloidin into live keratocytes for speckle staining of F-actin

Alexa Fluor 546 phalloidin was introduced into live migrating keratocytes directly, using a previously described small-volume electroporator [27]. Briefly, Alexa Fluor 546 phalloidin (A22283; Life Technologies, Carlsbad, CA) was dissolved in DMSO and then diluted 20 times with Ginzburg Fish Ringer's solution (111.3 mM NaCl, 3.35 mM KCl, 2.7 mM $CaCl_2$ and 2.3 mM $NaHCO_3$, pH 7.6) including 0.5 mM $MgSO_4$, resulting in final concentrations of 10 μM Alexa phalloidin and 5% DMSO. Two microliters of this electroporation medium was sucked into a commercially available 10-μl short tip of an auto-pipette. The tip was then inserted into the electroporation cuvette. The electroporation area of the cuvette is a 5×5×0.1 mm region with a pair of aluminum sheet electrodes placed on two of its sides. The cuvette was attached to the coverslip to which the cells had adhered by manually lowering the auto-pipette. Immediately after discharge of electroporation medium into the space enclosed by the cuvette, electric field pulses of 300 V/cm amplitude and 30 ms duration were applied three times from a 10,000-μF capacitor to the medium between the electrodes.

Fixed cell staining

Fixed cell staining was performed according to the methods described previously [29,30] with minor modifications. Briefly, cells were fixed with 4% paraformaldehyde for 15 min, permeabilized with 0.1% Triton X-100 for 10 min, and blocked with 0.2% gelatin for 30 min. The cells were then incubated with primary antibody: mouse monoclonal α-tubulin (1:4,000 dilution, T5168, Sigma-Aldrich) and Alexa Fluor 488 phalloidin (0.33 U/ml, A12379; Life Technologies) for 60 min. After several washes with 0.2% gelatin, the cells were incubated with secondary antibody: Alexa Fluor 546 Anti-mouse IgG (1:2,000 dilution, A-11030, Life Technologies) for 60 min. The fixation and staining were all carried out at room temperature. In the vinculin stain tests, mouse monoclonal vinculin (1:800 dilution, V9131, Sigma-Aldrich) and Alexa Fluor 546 Anti-mouse IgG (1:2,000 dilution, A-11030, Life Technologies) were used as the primary and secondary antibody, respectively. In the myosin IIA stain tests, the cells were permeabilized with 0.02% Triton X-100. Rabbit polyclonal myosin IIA (1:200 dilution, M8064, Sigma-Aldrich) and Alexa Fluor 546 Anti-rabbit IgG (1:2,000 dilution, A-11071, Life Technologies) were then used as primary and secondary antibody, respectively.

Microscopy

Fluorescence images of live and fixed cells were detected using an inverted microscope (Ti; Nikon, Tokyo, Japan) equipped with a laser confocal scanner unit (CSU-X1; Yokogawa, Tokyo, Japan) and an EM CCD camera (DU897; Andor, Belfast, UK) through a 100× objective lens (CFI Apo TIRF 100×H/1.49; Nikon).

Traction force microscopy

Traction force microscopy was performed according to the methods described previously [31,32] with minor modifications. A type of polydimethylsiloxane (PDMS) (CY52-276A and B; Dow Corning Toray, Tokyo, Japan) was used as

the material for the elastic sheet. CY52-276A and B were mixed at 6:10 in weight. A 40–45 mg aliquot of the mixture was spread on a 22×22 mm coverslip (No. 0, Matsunami, Osaka, Japan). After the mixture had hardened, the solidified substrata were kept in a hermetically sealed case with a 50-µl aliquot of liquid silane (3-aminopropyl triethoxysilane, Sigma-Aldrich) at 70°C for 1 hour, to attach the silane to the surface of the silicon substrata by vapor deposition. A round chamber, 16 mm in diameter × 2 mm in depth, was then assembled using the coated coverslip to form the bottom of the chamber. Red fluorescent carboxylate-modified microspheres (20 nm in diameter; peak excitation and emission wavelengths of 580 and 605 nm respectively; F-8786, Life Technologies) were attached to the surface of the substrata using the binding between the amino group in the silane and the carboxyl group in the microspheres.

The Young's Moduli of the elastic substrata were measured using the method of Lo and colleagues [33]. Briefly, a steel ball (0.5 mm diameter, 7.8 kg/dm^3) was placed on a substratum embedded with fluorescent beads. Young's Modulus was calculated as $Y=3(1-p^2)f^2/4d^{3/2}r^{1/2}$, where f is the force exerted on the sheet, d is the indentation, r is the radius of the steel ball, and p is the Poisson ratio [assumed to be 0.5 [34]]. Typical values of the Young's modulus was 13.8 kPa.

The image data were analyzed using ImageJ (http://rsbweb.nih.gov/ij). Images of fluorescent beads were first aligned to correct any experimental drift using StackReg, an ImageJ plug-in. The displacement field and the traction force field were then calculated using two plug-ins, PIV and FTTC [35]. The regularization parameter was set at 3×10^{-10} for all traction force reconstructions.

Results

Microtubule distribution, migration and cell shape of the nocodazole-treated keratocytes

To test whether microtubules were completely disrupted by the treatment with 10-µM nocodazole for 30 min, the cells were fixed immediately after the treatment. Tubulin and F-actin were then stained. Although microtubules are seen only in the cell body of the untreated cell (Fig. 1A), many small dots of tubulin were seen over the whole region of the nocodazole-treated cell (Fig. 1B). However, there were no significant differences in F-actin distribution between the untreated (Fig. 1C) and treated cells (Fig. 1D). These results indicate that microtubules are disrupted by the nocodazole treatment. We then compared the migration of untreated (Fig. 1E, Supplementary Movie S1) and nocodazole-treated cells (Fig. 1F, Supplementary Movie S2). Not only untreated cells, which were exposed to 0.1% DMSO, but also nocodazole-treated cells, which were exposed to 10 µg/ml nocodazole and 0.1% DMSO, continued their migration. There proved to be no significant difference, either in the migration velocity (Fig. 1L) or in the directionality (Fig. 1M) between untreated and nocodazole-treated cells, as shown in a previous study [25].

Next, to compare the cell shapes quantitatively, we defined the "curvature radius" and "center angle" of the leading edge (Fig. 1G). A circular arc was traced along the leading edge of the cell. The two points at which the arc departed from the leading edge were connected to the center (o in Fig. 1G) of the arc by straight lines. The lengths of the two lines and the angle between them were defined as the "curvature radius" and "center angle," respectively. Keratocytes do not constantly maintain the same shape while migrating [36,37]. Thus, we randomly selected bilaterally symmetric cells from images of all the migrating cells and measured their curvature radii and center angles (Fig. 1H–K). There proved to be no significant difference either in curvature radius ($p=0.440$, Fig 1H and I) or in center angle ($p=0.411$, Fig. 1J and K) between the untreated and nocodazole-treated cells.

Graded radial expansion of leading edge in the nocodazole-treated keratocytes

To reveal how the disruption of microtubules affected the molecular dynamics related to cell migration, we compared the rates of leading edge expansion and RF in untreated and nocodazole-treated cells. F-actin in the nocodazole-treated cells was stained by Alexa Fluor 546 phalloidin in a speckled fashion (Fig. 2A). Many small bright dots are clearly seen throughout the cells. To perform a quantitative analysis, the directions of "Middle" and "Side" in the cell were defined (Fig. 2B). Three dashed straight lines, by which the center angle was divided into four equal parts, were drawn. The directions of the middle and the right-hand dashed lines were defined as Middle and Side, respectively. From the sequential fluorescence images, rectangles, 12 µm in height and 2.7 µm in width, along the Middle and Side directions ("*m*" and "*s*" in Fig. 2A) were cropped and aligned sequentially to construct kymographs (Fig. 2C and D). In the kymographs, the leading edge moved forward (dashed arrow in Fig. 2C and D), while the dots show retrograde movement (arrow in Fig. 2C and D). The expansion rate of the leading edge (left columns in Fig. 2E and H) and the RF rate (left columns in Fig. 2F and I) were estimated from the kymographs. AP rates (left columns in Fig. 2G and J) were calculated as their sum. These values were also measured in the untreated cells (right columns in Fig. 2E–J). There was no significant difference in any of the rates at the Middle and Side between nocodazole-treated and untreated cells.

Vinculin distribution in the nocodazole-treated keratocytes

Distributions of vinculin, a focal adhesion protein, in the untreated and the nocodazole-treated cells visualized by immunofluorescent staining are shown in Figure 3A and B. The relative fluorescence intensities of vinculin in the untreated and the nocodazole-treated cells were calculated by dividing the intensity at each point (*a* in Fig. 3C inset) around the cell perimeter by the maximum one in the cell.

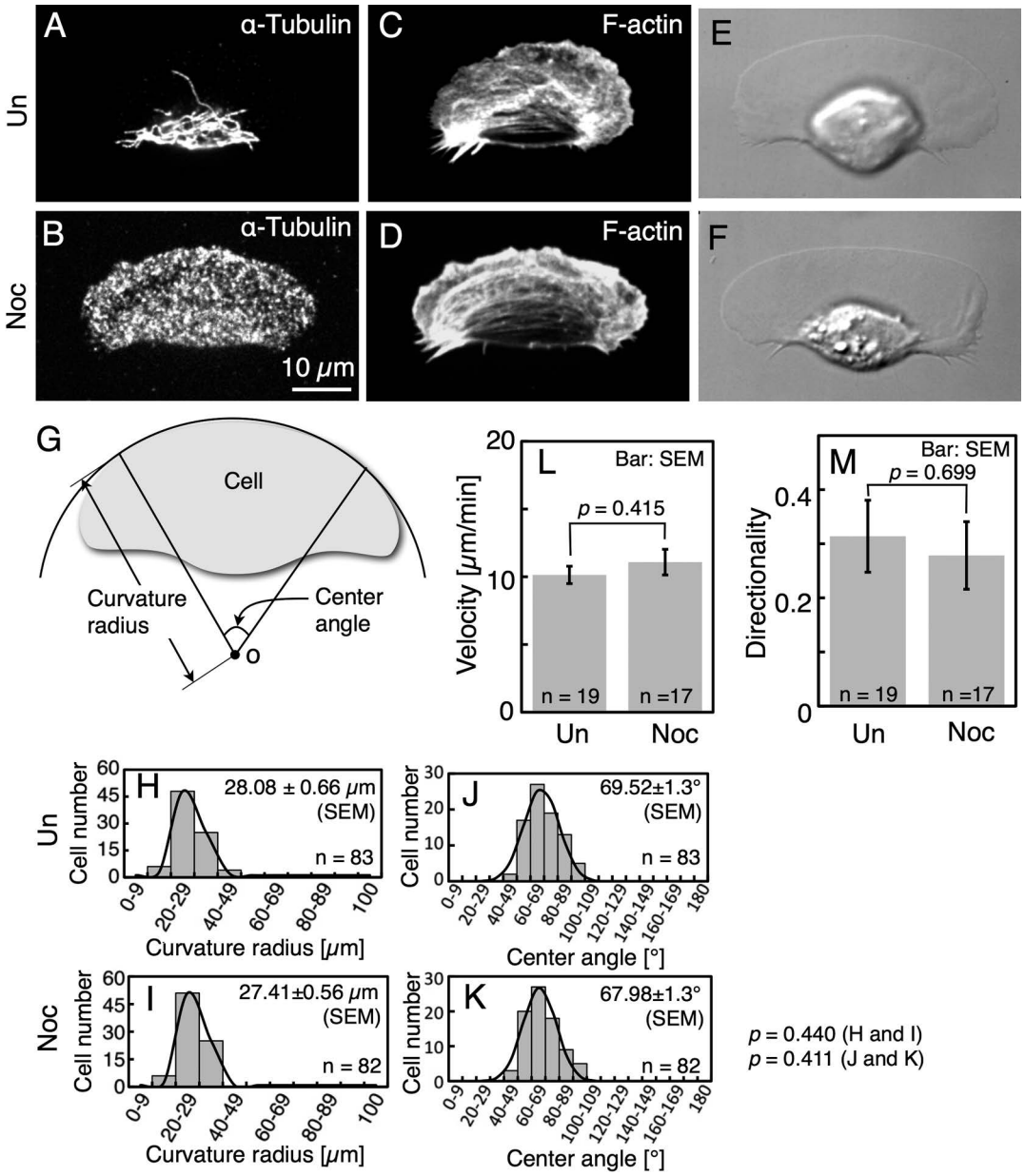

Figure 1 Nocodazole disrupts microtubules but does not affect migration or cell shape. (A) α-Tubulin in an untreated cell. (B) α-Tubulin in a nocodazole-treated cell. (C and D) F-actin in cells, the same as A and B, respectively. (E and F) DIC images of the untreated cell (E) and the nocodazole-treated cell (F). A, C & E, and B, D & F are typical of 19 and 17 cells, respectively. (G) Definition of "curvature radius" and "center angle" of the leading edge. See text for full details. (H and I) Frequency distributions of curvature radius of the untreated cells (H) and nocodazole-treated cells (I). (J and K) Frequency distributions of the center angle of the untreated cells (J) and nocodazole-treated cells (K). (L and M) Migration velocity (L) and directionality (M) of the untreated cells (left) and the nocodazole-treated cells (right). Directionality was defined as the displacement over 30 min divided by the total path length of the cell. Noc and Un in each panel mean nocodazole-treated cells and untreated cells, respectively.

The blue and red lines in Figure 3C, which respectively indicate the untreated and the nocodazole-treated cells, almost completely overlap each other. The regions in which the fluorescence intensity of vinculin exceeded 30% of the maximum intensity in the cell were limited to the rear left and the right ends of the cell (the green ellipses in Fig. 3A and B). We concluded these areas to be the region of rear focal adhesions. The ratio of the area of the regions to the whole cell area was then calculated (Fig. 3D). There was no significant difference in the vinculin distribution between the untreated and the nocodazole-treated cells, suggesting that the distribution of focal adhesions is not affected by disruption of the microtubules.

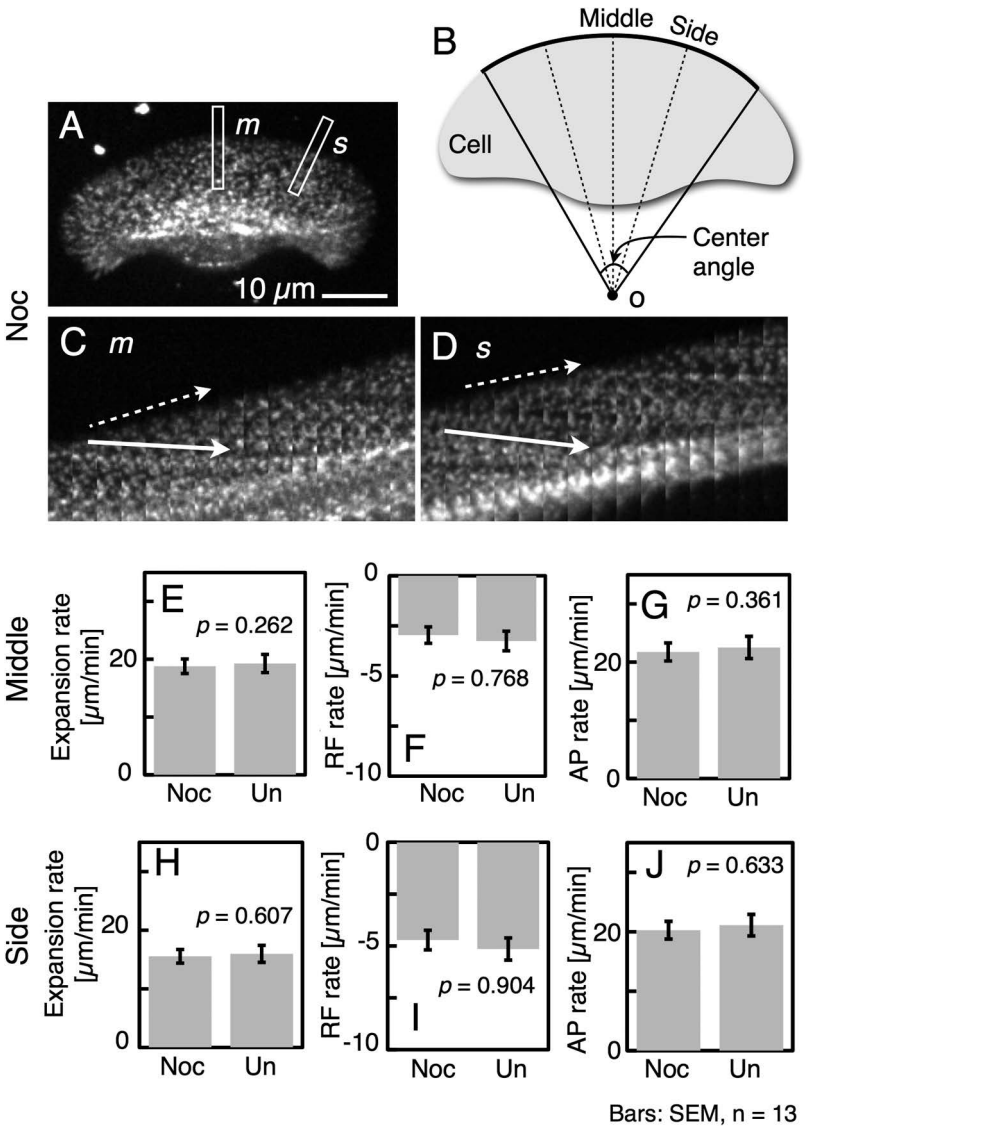

Figure 2 Nocodazole does not affect the rates of leading edge extension, RF and AP. (A) Single fluorescence image of a migrating nocodazole-treated cell selected from consecutive images. The image is typical of 13 cells. (B) Definition of the directions of "Middle" and "Side." See text for full details. Kymographs (C and D) were constructed from image strips (white rectangles labeled respectively as *m* and *s* in A) taken from consecutive images. Forward movement of the cell edge is indicated in the kymographs with dotted arrows, and RF is indicated with arrows. (E–G) Expansion rate of the leading edge (E), the RF rate (F) and the AP rate (G) at the Middle of nocodazole-treated cells (left columns) and of untreated cells (right columns). (H–J) Expansion rate of the leading edge (H), the RF rate (I) and the AP rate (J) at the Side of nocodazole-treated cells (left columns) and of untreated cells (right columns). The values of left columns in E and F, and H and I were estimated from the kymographs (C and D). Those in G and J were calculated as the sum of those in E and F, and H and I, respectively. Noc and Un in each panel mean nocodazole-treated cells and untreated cells, respectively. The *p*-values were calculated using Student's t-test.

Myosin IIA distribution in the nocodazole-treated keratocytes

The distribution of myosin IIA in the untreated and nocodazole-treated cells, visualized by immunofluorescent staining, is shown in Figure 4A and B. In both cells, myosin IIA appears to have accumulated mainly near the left and the right edges of the cell body in the lamellipodium. To compare the accumulation quantitatively, two rectangles, α and β, were defined (Fig. 4C). α was in the Middle direction as defined in Figure 2B. The top and the bottom of α are on the leading edge and on the top of the cell body, respectively. β was on the line from the center (o in Fig. 4C) of the arc to the right edge of the cell body. The top and the bottom of β are respectively on the leading edge and on the edge of the cell body. The width of both rectangles was 5 μm. Myosin II density in α and β was calculated by dividing the area where fluorescence intensity exceeded 40% of the maximum intensity in the cell by the area of the rectangles. The density ratio

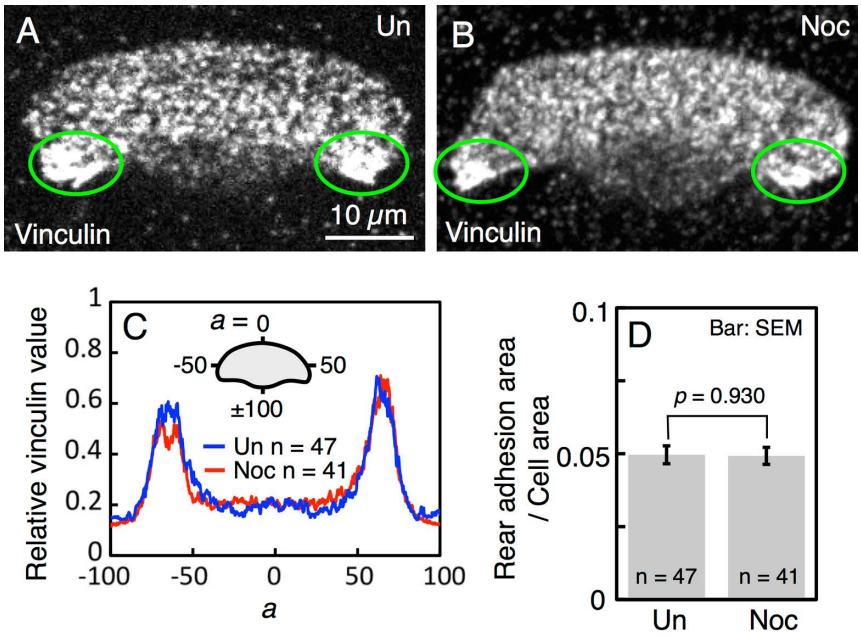

Figure 3 Distribution of vinculin in untreated cells and nocodazole-treated cells. (A and B) Immunofluorescence staining of vinculin in an untreated cell (A) and a nocodazole-treated cell (B). The images A and B are typical of 47 and 41 cells, respectively. (C) Averaged relative fluorescence intensities of vinculin in the untreated cells (blue) and the nocodazole-treated ones (red). The values were calculated by dividing the intensity at each point (*a* in inset) around the cell perimeter by the maximum intensity within the cell. (D) The ratio of the area of rear focal adhesions to the whole cell area. Left: untreated cells. Right: nocodazole-treated cells. The focal adhesion-region (green ellipses in A and B) was defined as that at which the fluorescent intensity of vinculin was higher than 30% of the maximum intensity in the cell. Noc and Un in each panel mean nocodazole-treated cells and untreated cells, respectively.

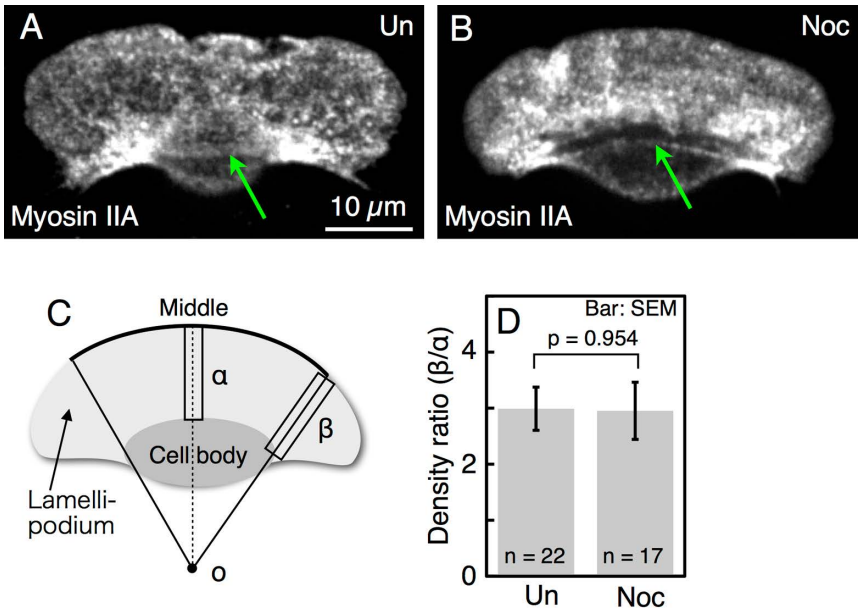

Figure 4 Distribution of myosin IIA in untreated and nocodazole-treated cells. (A and B) Immunofluorescence staining of myosin IIA in an untreated (A) and a nocodazole-treated cell (B). Green arrows: stress fibers. Images A and B are typical of 22 and 17 cells, respectively. (C) Definition of two regions, α and β, to compare the accumulation of myosin IIA quantitatively. See text for full details. (D) Density ratio of myosin II, calculated by dividing the density in β by that in α in C. Left: untreated cells; Right: nocodazole-treated cells. The density of myosin II was calculated by dividing the area in which fluorescence intensity was higher than 40% of the maximum intensity within the cell by the area of α or β. Noc and Un in each panel mean nocodazole-treated cells and untreated cells, respectively.

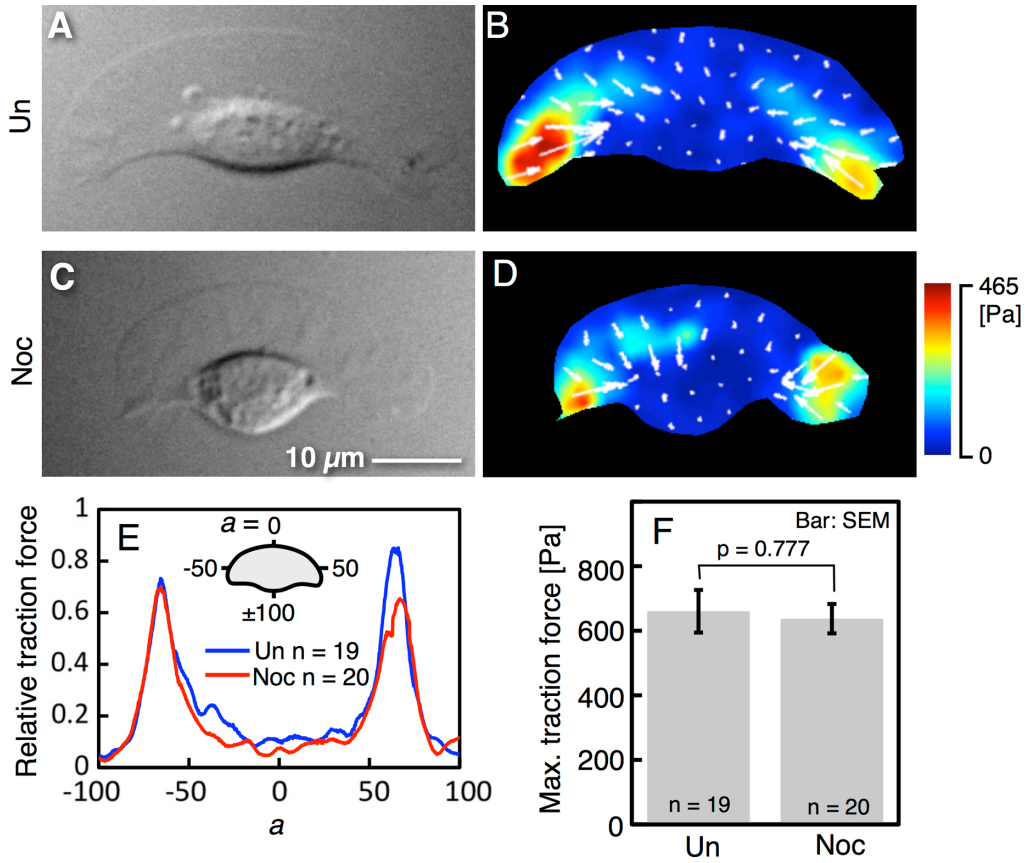

Figure 5 Traction forces exerted by untreated cells and nocodazole-treated cells. (A and B) An untreated cell (A) and its traction forces (B). (C and D) A nocodazole-treated cell (C) and its traction forces (D). Direction and length of white arrows in B and D respectively indicate the direction and the relative magnitude of traction forces at the base of the arrows. The images A & B and C & D are typical of 19 and 20 cells, respectively. (E) Average relative traction forces in untreated cells (blue) and nocodazole-treated cells (red). These values were calculated by dividing the force at each point (*a* in inset) around the cell perimeter by the maximum force in the cell. (F) Maximum traction forces in untreated cells (left) and nocodazole-treated cells (right). Noc and Un in each panel mean nocodazole-treated cells and untreated cells, respectively.

of myosin II was then calculated by dividing the density in β by that in α. There proved to be no significant difference in the density ratio of myosin II between the untreated and the nocodazole-treated cells (Fig. 4D), suggesting that the distribution of myosin II is not affected by the disruption of microtubules.

Traction forces exerted by the nocodazole-treated keratocytes

Contractile forces exerted by the stress fibers (the green arrows in Fig. 4A and B) appear to be transmitted to the substratum as traction forces through focal adhesions in the left and right ends of the cell (ellipses in Fig. 3A and B). Next, we measured the traction forces exerted by the untreated (Fig. 5A, B and Supplementary Movie S3) and nocodazole-treated cells (Fig. 5C, D and Supplementary Movie S4). In the untreated cell, traction forces were exerted mainly at the left and right ends of the cell (Fig. 5B) as revealed in previous studies [38–42]. In the nocodazole-treated cell too, traction forces were exerted there (Fig. 5D). The relative traction forces in the untreated and the nocodazole-treated cells were calculated by dividing the force at each point (*a* in Fig. 5E inset) around the cell perimeter by the maximum force within the cell. The blue and red lines in Figure 5E, which indicate the untreated and the nocodazole-treated cells, respectively, almost completely overlap each other. Figure 5F shows the maximum traction force in the cells. There is no significant difference between the untreated and the nocodazole-treated cells, suggesting that traction forces are similarly not affected by disruption of the microtubules in keratocytes.

Discussion

In this study, nocodazole treatment did not affect the migration velocity, directionality or shape of the leading edge (Fig. 1), RF rate (Fig. 2), distribution of vinculin (Fig. 3) or myosin II (Fig. 4), or the traction forces (Fig. 5), in spite of it having depolymerized the microtubules (Fig. 1B). As a source of traction forces, stress fibers can be seen in

both untreated and nocodazole-treated keratocytes (Fig. 4A and B). These results suggest that microtubules do not regulate the intracellular molecular dynamics of crawling migration of keratocytes.

What are the minimal required processes for cell migration? Simplified physical model of a crawling cell [43] suggests that only actin polymerization and focal adhesions are required for the most simple crawling migration. To generate variations of shapes of migrating cells including the crescent-shape of keratocytes, contraction of actomyosin is also required. In the model, cellular motility exploits autonomous physical mechanisms whose operation does not need continuous regulatory effort by microtubules.

In fact, in all cell types, actin polymerization and actomyosin contraction do not require microtubules *per se* [13]. Then, what is the role of microtubules in cell migration? It may be to manage the overall organization and positioning of multiple activities within the cell whose actin-rich region is apart from the cell body [44]. Microtubule dynamics are responsible for the forward translocation of neuronal growth cones [45]. In nerve cells, the actin-rich region is limited to the peripheral zone of the growth cone. The growth cone is separated from the cell body by an axon. Microtubules extend from the cell body into the central region of the growth cone, and connect the cell body and the actin-rich peripheral zone in the growth cone.

On the other hand, keratocytes have a large crescent-shaped lamellipodium. The actin-rich region is not limited to the peripheral zone of the lamellipodium but spreads out in the whole lamellipodium. The cell body of the keratocyte is just behind the actin-rich lamellipodium. Moreover, the expansion rate of the leading edge is constant, because the shape of the leading edge does not change during migration. Thus, in keratocytes, it may not be necessary to manage the exact positioning of expansion of the leading edge. It is possible that neither actin polymerization, nor actomyosin contraction, nor disassembly of the dot-like adhesions in keratocytes [46] require additional microtubule-introduced stimuli, although microtubules grow directionally toward the target focal adhesions, which leads to their disassembly in fibroblasts [47–49].

In fibroblasts, not only microtubules but also nucleus plays an important role for normal cell motility [50]. Actomyosin contractile forces are transmitted from the front to the back of the cell through the nucleus to detach the trailing edge. However, keratocyte fragments without a nucleus also migrate in the same way as the original cell, indicating that not even a nucleus is required for migration in keratocytes. To reveal the minimal requirement for cell migration experimentally is an interesting future area of study.

Conclusion

Many processes essential to migration are regulated by microtubules in many cells, including fibroblasts and neurons. In the present study, however, we suggest microtubules are not required for crawling migration of keratocytes, and are not an essential part of intracellular molecular dynamics.

Acknowledgements

We thank Dr. H. Miyoshi (Riken, Wako, Japan) for instruction on cell fixation and staining, and Dr. T. Mizuno (AIST, Tsukuba, Japan) for instruction on live cell preparation. YI was supported by MEXT Kakenhi Grants Nos. 26103524, 26650050 and 15H01323.

Competing interests

The authors declare no competing interests.

Author contributions

H. N. performed the experiments and data analysis; C. O. and Y. I. devised the experiments, coordinated the research, and wrote the manuscript.

References

[1] Lauffenburger, D. A. & Horwitz, A. F. Cell migration: a physically integrated molecular process. *Cell* **84**, 359–369 (1996).
[2] Ridley, A. J., Schwartz, M. A., Burridge, K., Firtel, R. A., Ginsberg, M. H., Borisy, G. *et al.* Cell migration: integrating signals from front to back. *Science* **302**, 1704–1709 (2003).
[3] Raftopoulou, M. & Hall, A. Cell migration: Rho GTPases lead the way. *Dev. Biol.* **265**, 23–32 (2004).
[4] Reid, B., Song, B., McCaig, C. D. & Zhao, M. Wound healing in rat cornea: the role of electric currents. *FASEB J.* **19**, 379–386 (2005).
[5] Zhao, M., Song, B., Pu, J., Wada, T., Reid, B., Tai, G. *et al.* Electrical signals control wound healing through phosphatidylinositol-3-OH kinase-γ and PTEN. *Nature* **442**, 457–460 (2006).
[6] Parent, C. A. Making all the right moves: chemotaxis in neutrophils and *Dictyostelium*. *Curr. Opin. Cell Biol.* **16**, 4–13 (2004).
[7] Friedl, P. & Alexander, S. Cancer invasion and the microenvironment: plasticity and reciprocity. *Cell* **147**, 992–1009 (2011).
[8] Svitkina, T. M., Verkhovsky, A. B., McQuade, K. M. & Borisy, G. G. Analysis of the actin-myosin II system in fish epidermal keratocytes: mechanism of cell body translocation. *J. Cell Biol.* **139**, 397–415 (1997).
[9] Wang, Y. L. Exchange of actin subunits at the leading edge of living fibroblasts: possible role of treadmilling. *J. Cell Biol.* **101**, 597–602 (1985).
[10] Jay, P. Y., Pham, P. A., Wong, S. A. & Elson, E. L. A mechanical function of myosin II in cell motility. *J. Cell Sci.* **108**, 387–393 (1995).
[11] Chen, W. T. Mechanism of retraction of the trailing edge during fibroblast movement. *J. Cell Biol.* **90**, 187–200 (1981).
[12] Vasiliev, J. M., Gelfand, I. M., Domnina, L. V., Ivanova, O. Y., Komm, S. G. & Olshevskaja, L. V. Effect of colcemid on the locomotory behaviour of fibroblasts. *J. Embryol. Exp. Morphol.* **24**, 625–640 (1970).
[13] Kaverina, I. & Straube, A. Regulation of cell migration by dynamic microtubules. *Semin. Cell Dev. Biol.* **22**, 968–974 (2011).

[14] Akhshi, T. K., Wernike, D. & Piekny, A. Microtubules and actin crosstalk in cell migration and division. *Cytoskeleton* **71**, 1–23 (2014).
[15] Brandt, D. T. & Grosse, R. Get to grips: steering local actin dynamics with IQGAPs. *EMBO Rep.* **8**, 1019–1023 (2007).
[16] Amano, M., Nakayama, M. & Kaibuchi, K. Rho-kinase/ROCK: a key regulator of the cytoskeleton and cell polarity. *Cytoskeleton* **67**, 545–554 (2010).
[17] Waterman-Storer, C. M., Worthylake, R. A., Liu, B. P., Burridge, K. & Salmon, E. D. Microtubule growth activates Rac1 to promote lamellipodial protrusion in fibroblasts. *Nat. Cell Biol.* **1**, 45–50 (1999).
[18] Montenegro-Venegas, C., Tortosa, E., Rosso, S., Peretti, D., Bollati, F., Bisbal, M. *et al.* MAP1B regulates axonal development by modulating Rho-GTPase Rac1 activity. *Mol. Biol. Cell* **21**, 3518–3528 (2010).
[19] Rooney, C., White, G., Nazgiewicz, A., Woodcock, S. A., Anderson, K. I., Ballestrem, C. *et al.* The Rac activator STEF (Tiam2) regulates cell migration by microtubule-mediated focal adhesion disassembly. *EMBO Rep.* **11**, 292–298 (2010).
[20] Chang, Y.-C., Nalbant, P., Birkenfeld, J., Chang, Z.-F. & Bokoch, G. M. GEF-H1 couples nocodazole-induced microtubule disassembly to cell contractility via RhoA. *Mol. Biol. Cell* **19**, 2147–2153 (2008).
[21] Krendel, M., Zenke, F. T. & Bokoch, G. M. Nucleotide exchange factor GEF-H1 mediates cross-talk between microtubules and the actin cytoskeleton. *Nat. Cell Biol.* **4**, 294–301 (2002).
[22] Enomoto, T. Microtubule disruption induces the formation of actin stress fibers and focal adhesions in cultured cells: possible involvement of the rho signal cascade. *Cell Struct. Funct.* **21**, 317–326 (1996).
[23] Nalbant, P., Chang, Y.-C., Birkenfeld, J., Chang, Z.-F. & Bokoch, G. M. Guanine nucleotide exchange factor-H1 regulates cell migration via localized activation of RhoA at the leading edge. *Mol. Biol. Cell* **20**, 4070–4082 (2009).
[24] Keren, K., Pincus, Z., Allen, G. M., Barnhart, E. L., Marriott, G., Mogilner, A. *et al.* Mechanism of shape determination in motile cells. *Nature* **453**, 475–480 (2008).
[25] Euteneuer, U. & Schliwa, M. Persistent, directional motility of cells and cytoplasmic fragments in the absence of microtubules. *Nature* **310**, 58–61 (1984).
[26] Verkhovsky, A. B., Svitkina, T. M. & Borisy, G. G. Self-polarization and directional motility of cytoplasm. *Curr. Biol.* **9**, 11–20 (1999).
[27] Tsugiyama, H., Okimura, C., Mizuno, T. & Iwadate, Y. Electroporation of adherent cells with low sample volumes on a microscope stage. *J. Exp. Biol.* **216**, 3591–3598 (2013).
[28] Mizuno, T. & Sekiguchi, Y. Staurosporine induces lamellipodial widening in locomoting fish keratocytes by abolishing the gradient from radial extension of leading edge. *BIOPHYSICS* **7**, 69–75 (2011).
[29] Miyoshi, H. & Adachi, T. Spatiotemporal coordinated hierarchical properties of cellular protrusion revealed by multiscale analysis. *Integr. Biol. Quant. Biosci. Nano Macro* **4**, 875–888 (2012).
[30] Okeyo, K. O., Adachi, T., Sunaga, J. & Hojo, M. Actomyosin contractility spatiotemporally regulates actin network dynamics in migrating cells. *J. Biomech.* **42**, 2540–2548 (2009).
[31] Iwadate, Y. & Yumura, S. Actin-based propulsive forces and myosin-II-based contractile forces in migrating *Dictyostelium* cells. *J. Cell Sci.* **121**, 1314–1324 (2008).
[32] Iwadate, Y. & Yumura, S. Molecular dynamics and forces of a motile cell simultaneously visualized by TIRF and force microscopies. *Biotechniques* **44**, 739–750 (2008).
[33] Lo, C. M., Wang, H. B., Dembo, M. & Wang, Y. L. Cell movement is guided by the rigidity of the substrate. *Biophys. J.* **79**, 144–152 (2000).
[34] Dembo, M., Oliver, T., Ishihara, A. & Jacobson, K. Imaging the traction stresses exerted by locomoting cells with the elastic substratum method. *Biophys. J.* **70**, 2008–2022 (1996).
[35] Tseng, Q., Duchemin-Pelletier, E., Deshiere, A., Balland, M., Guillou, H., Filhol, O. *et al.* Spatial organization of the extracellular matrix regulates cell-cell junction positioning. *Proc. Natl. Acad. Sci. USA* **109**, 1506–1511 (2012).
[36] Barnhart, E. L., Lee, K.-C., Keren, K., Mogilner, A. & Theriot, J. A. An adhesion-dependent switch between mechanisms that determine motile cell shape. *PLoS Biol.* **9**, e1001059 (2011).
[37] Barnhart, E. L., Allen, G. M., Jülicher, F. & Theriot, J. A. Bipedal locomotion in crawling cells. *Biophys. J.* **98**, 933–942 (2010).
[38] Fournier, M. F., Sauser, R., Ambrosi, D., Meister, J.-J. & Verkhovsky, A. B. Force transmission in migrating cells. *J. Cell Biol.* **188**, 287–297 (2010).
[39] Jurado, C., Haserick, J. R. & Lee, J. Slipping or gripping? Fluorescent speckle microscopy in fish keratocytes reveals two different mechanisms for generating a retrograde flow of actin. *Mol. Biol. Cell* **16**, 507–518 (2005).
[40] Doyle, A., Marganski, W. & Lee, J. Calcium transients induce spatially coordinated increases in traction force during the movement of fish keratocytes. *J. Cell Sci.* **117**, 2203–2214 (2004).
[41] Burton, K., Park, J. H. & Taylor, D. L. Keratocytes generate traction forces in two phases. *Mol. Biol. Cell* **10**, 3745–3769 (1999).
[42] Chen, Z., Lessey, E., Berginski, M. E., Cao, L., Li, J., Trepat, X. *et al.* Gleevec, an Abl family inhibitor, produces a profound change in cell shape and migration. *PloS One* **8**, e52233 (2013).
[43] Tjhung, E., Tiribocchi, A., Marenduzzo, D. & Cates, M. E. A minimal physical model captures the shapes of crawling cells. *Nat. Commun.* **6**, 5420 (2015).
[44] Etienne-Manneville, S. Actin and microtubules in cell motility: which one is in control? *Traffic* **5**, 470–477 (2004).
[45] Tanaka, E., Ho, T. & Kirschner, M. W. The role of microtubule dynamics in growth cone motility and axonal growth. *J. Cell Biol.* **128**, 139–155 (1995).
[46] Anderson, K. I. & Cross, R. Contact dynamics during keratocyte motility. *Curr. Biol.* **10**, 253–260 (2000).
[47] Bershadsky, A., Chausovsky, A., Becker, E., Lyubimova, A. & Geiger, B. Involvement of microtubules in the control of adhesion-dependent signal transduction. *Curr. Biol.* **6**, 1279–1289 (1996).
[48] Liu, B. P., Chrzanowska-Wodnicka, M. & Burridge, K. Microtubule depolymerization induces stress fibers, focal adhesions, and DNA synthesis via the GTP-binding protein Rho. *Cell Adhes. Commun.* **5**, 249–255 (1998).
[49] Kaverina, I., Rottner, K. & Small, J. V. Targeting, capture, and stabilization of microtubules at early focal adhesions. *J. Cell Biol.* **142**, 181–190 (1998).
[50] Wu, J., Kent, I. A., Shekhar, N., Chancellor, T. J., Mendonca, A., Dickinson, R. B. *et al.* Actomyosin pulls to advance the nucleus in a migrating tissue cell. *Biophys. J.* **106**, 7–15 (2014).